International Forum on Aeroelasticity and Structural Dynamics
IFASD 2017
25-28 June 2017 Como, Italy

A METHOD FOR PREDICTING MULTIVARIATE RANDOM LOADS AND A DISCRETE APPROXIMATION OF THE MULTIDIMENSIONAL DESIGN LOAD ENVELOPE

Carlo Aquilini[1] **and Daniele Parisse**[1]

[1]Airbus Defence and Space GmbH
Rechliner Str., 85077 Manching, Germany
carlo.aquilini@airbus.com

Keywords: aeroelasticity, buffeting, combined random loads, multidimensional design load envelope, IFASD-2017

Abstract: Random loads are of greatest concern during the design phase of new aircraft. They can either result from a stationary Gaussian process, such as continuous turbulence, or from a random process, such as buffet. Buffet phenomena are especially relevant for fighters flying in the transonic regime at high angles of attack or when the turbulent, separated air flow induces fluctuating pressures on structures like wing surfaces, horizontal tail planes, vertical tail planes, airbrakes, flaps or landing gear doors.
In this paper a method is presented for predicting n-dimensional combined loads in the presence of massively separated flows. This method can be used both early in the design process, when only numerical data are available, and later, when test data measurements have been performed. Moreover, the two-dimensional load envelope for combined load cases and its discretization, which are well documented in the literature, are generalized to n dimensions, $n \geq 3$.

1 INTRODUCTION

The main objectives of this paper are:

1. To derive a method for predicting multivariate loads (but also displacements, velocities and accelerations in terms of auto- and cross-power spectra, [1, pp. 319-320]) for aircraft, or parts of them, subjected to a random excitation.
2. To investigate the geometrical shape of the load envelope and to discretize it in order to obtain a finite number of design load cases. The load envelope shall be considered as n-dimensional.

The aforementioned method is derived for wide-sense stationary stochastic processes (see [1, pp. 297-298]). The starting point is the availability of the unsteady, motion-independent pressure distribution on a three-dimensional aerodynamic grid (either from CFD or from test measurements, obtained in flight or in wind tunnel) and a structural model, usually an FEM statically condensed with a Guyan reduction (see [2]) to which the masses are added separately. Depending on the nature of the problem, the self-induced aerodynamic forces could also have an important impact on the structural response and they are, therefore, to be included in the formulation. An industry standard within the field of the linear methods for the determination of the generalized aerodynamic forces is the doublet-lattice method (see [3]).
The aerodynamic pressure distribution is integrated obtaining a force distribution statically

equivalent on the same grid (section 2). Surface splines are then used in order to interpolate the force distribution, obtaining an equivalent system on the structural grid (section 3). The aeroelastic response of the structure to the unsteady flow excitation (namely *buffeting*) is computed in modal space using a stochastic approach (section 4).
With the obtained results, it is possible to define an n-dimensional load envelope. It contains equally probable combinations of loads between their minimum and maximum values. Although the load envelope is n-dimensional (because it generally represents combinations of at most three forces and three moments at multiple monitoring stations), only the two- and three-dimensional cases have been studied thoroughly in the literature (cf. [4–6]). Furthermore, to the best of the authors' knowledge, a general method for discretizing the n-dimensional loads envelope for $n \geq 3$ is missing. Therefore, after determining the geometrical shape of the load envelope for Gaussian distributed combined loads (an ellipse for $n = 2$, an ellipsoid for $n = 3$ and an n-dimensional ellipsoid for $n \geq 4$), a new method for discretizing the load envelope is introduced. The specific cases for two and three dimensions are first presented, and then the general n-dimensional case valid for all $n \geq 2$ is derived (section 5). This method consists in circumscribing the ellipsoid with a convex polytope, obtained by a transformation of the n-dimensional generalization of one of the 13 Archimedean solids, the small rhombicuboctahedron. The vertices of this polytope provide a finite number of design load cases and they can generally be applied for every problem where the external random excitation induces multivariate random loads; example of such problems are buffeting or continuous turbulence response.

2 THE EXTERNAL AERODYNAMIC EXCITATION

Let the unsteady, motion-independent pressure distribution be available on a three-dimensional grid from CFD or test measurements. Aim of this section is to show how to integrate the pressure distribution obtaining a force distribution statically equivalent on the same mesh. If the force distribution is already available, it is possible to proceed directly with the interpolation of the aerodynamic forces over the structural mesh, as explained in section 3.
Let us consider an unstructured or regular mesh, where the generic r-th cell has c vertices, with $c = 3$ for unstructured meshes and $c = 4$ for structured ones.
It is possible to integrate the pressure distribution over the r-th cell as

$$\begin{cases} F_{z_r} = \iint p_r(x,y)\,\mathrm{d}x\mathrm{d}y \\ M_{x_r} = \iint (y - y_{r_{ref}}) p_r(x,y)\,\mathrm{d}x\mathrm{d}y \\ M_{y_r} = -\iint (x - x_{r_{ref}}) p_r(x,y)\,\mathrm{d}x\mathrm{d}y \end{cases} \tag{1}$$

where $p_r(x,y)$ is the pressure distribution over the r-th cell, $(y - y_{r_{ref}})$ and $(x - x_{r_{ref}})$ are the lever arms from the arbitrary reference point $(x_{r_{ref}}, y_{r_{ref}})$, F_{z_r} is the resulting normal force along the local z_r-axis, M_{x_r} and M_{y_r} are the resulting moments about the local x_r- and y_r-axes. This methodology can be followed indistinctly in time or frequency domain and therefore the integration will be performed for each time or frequency step.
The resulting normal force and moments can be calculated also from the nodal forces as

$$\begin{cases} F_{z_r} = \sum_{i=1}^{c} f_{z_{r_i}} \\ M_{x_r} = \sum_{i=1}^{c} (y_{r_i} - y_{r_{ref}}) f_{z_{r_i}} \\ M_{y_r} = -\sum_{i=1}^{c} (x_{r_i} - x_{r_{ref}}) f_{z_{r_i}} \end{cases} \tag{2}$$

where $f_{z_{r_i}}$ are the normal forces at each i-th vertex of the cell and $(y_{r_i} - y_{r_{ref}})$ and $(x_{r_i} - x_{r_{ref}})$ are their lever arms from the arbitrary reference point $(x_{r_{ref}}, y_{r_{ref}})$. The systems in Eqs. (1) and (2) must be equal in order to obtain two distributions that are statically equivalent. Therefore, chosen a numerical method for integrating Eqs. (1) and expressing them in matrix form, we obtain

$$\mathbf{C}_{2_r}\mathbf{p}_r = \left[F_{z_r}, M_{x_r}, M_{y_r}\right]^\intercal = \mathbf{C}_{1_r}\mathbf{f}_{z_r} \tag{3}$$

where $\mathbf{f}_{z_r} = [f_{z_{r_1}}, \ldots, f_{z_{r_c}}]^\intercal$ and $\mathbf{p}_r = [p_{r_1}, \ldots, p_{r_c}]^\intercal$ are the nodal normal forces and the nodal pressures at the c vertices of the r-th cell, respectively.
Finally, $\mathbf{f}_{z_r}$ can be explicitly calculated as

$$\mathbf{f}_{z_r} = \mathbf{C}_{1_r}^{+}\mathbf{C}_{2_r}\mathbf{p}_r = \mathbf{A}_r\mathbf{p}_r \tag{4}$$

where $\mathbf{A}_r = \mathbf{C}_{1_r}^{+}\mathbf{C}_{2_r}$ and $\mathbf{C}_{1_r}^{+}$ is the Moore-Penrose pseudoinverse of $\mathbf{C}_{1_r}$ (cf. [7, pp. 44-59]). $\mathbf{C}_{1_r}$ and $\mathbf{C}_{2_r}$ are $3 \times c$ matrices and of full rank if the mesh is unstructured (with triangular cells), otherwise rectangular with more columns than rows. Therefore, $\mathbf{A}_r$ is a $c \times c$ matrix.
Let us denotate with $\mathbf{n}_r = [n_{r_X}, n_{r_Y}, n_{r_Z}]^\intercal$ the normal versor of the r-th cell, where n_{r_X}, n_{r_Y} and n_{r_Z} are its three components in the global reference system. It is possible to project the matrix $\mathbf{A}_r$ over the normal versor on all the vertices, such as

$$\mathbf{A}_{n_r} = \mathrm{diag}(\mathbf{n}_r, \ldots, \mathbf{n}_r)\mathbf{A}_r \tag{5}$$

where $\mathrm{diag}(\mathbf{n}_r, \ldots, \mathbf{n}_r)$ is a $3c \times c$ matrix.
The element matrices $\mathbf{A}_{n_r}$ can be merged by expanding each matrix in conformity with the global size of the aerodynamic mesh, obtaining $\mathbf{A}_{n_r}^e$, and by adding them together as

$$\mathbf{A}_n = \sum_{r=1}^{R} \mathbf{A}_{n_r}^e \tag{6}$$

Let us denotate with $\mathbf{p}_k$ the pressure distribution on the overall aerodynamic grid. It is now possible to compute the force distribution $\mathbf{f}_k$ on the same grid as

$$\mathbf{f}_k = \mathbf{A}_n\mathbf{p}_k \tag{7}$$

If $\mathbf{S}_{p_k}(j\omega)$ is the spectrum of $\mathbf{p}_k$, then the spectrum of $\mathbf{f}_k$ is given by (cf. [1, pp. 324 and 329])

$$\mathbf{S}_{f_k}(j\omega) = \mathbf{A}_n\mathbf{S}_{p_k}(j\omega)\mathbf{A}_n^\intercal \tag{8}$$

3 INTERCONNECTION OF STRUCTURE AND AERODYNAMICS

Once the force distribution over the aerodynamic mesh is available, it is necessary to project it on the structural mesh, since they generally do not coincide. There are several methods available in the literature for interpolating functions of two or three variables. One option is to use the surface splines based upon the small deflection equation of a plate (see [8–10] for the infinite plate spline method and [11, pp. 85-100] for the thin-plate spline method). This transformation satisfies the structural equivalence, i.e. the two force systems on the aerodynamic and on the structural grids will produce the same structural deflections. The splining method leads to the transformation matrix $\mathbf{G}_{kg}$, such as

$$\mathbf{u}_k = \mathbf{G}_{kg}\mathbf{u}_g \tag{9}$$

where $\mathbf{u}_k$ are the deflections of the aerodynamic grid and $\mathbf{u}_g$ are the deflections of the structural grid. Since the forces on the aerodynamic grid $\mathbf{f}_k$ and on the structural grid $\mathbf{f}_g$ produce the same virtual work, we obtain

$$\mathbf{f}_g = \mathbf{G}_{kg}^{\intercal}\mathbf{f}_k \tag{10}$$

$\mathbf{f}_k$ is expressed by the Eq. (7) in the form $[f_{k_{X1}}, f_{k_{Y1}}, f_{k_{Z1}}, \ldots, f_{k_{XN}}, f_{k_{YN}}, f_{k_{ZN}}]^{\intercal}$ and, for consistency, we rewrite Eq. (10) as

$$\mathbf{f}_g = (\mathbf{G}_{kg}^{\intercal} \otimes \mathbf{I}_3)\mathbf{f}_k \tag{11}$$

where $\otimes$ is the Kronecker product and $\mathbf{I}_3$ is the 3×3 identity matrix (cf. [7, pp. 22-24]).
At this point it is possible to interpolate the spectra of the aerodynamic forces on the structural grid as

$$\mathbf{S}_{f_g}(j\omega) = (\mathbf{G}_{kg}^{\intercal} \otimes \mathbf{I}_3)\mathbf{S}_{f_k}(j\omega)(\mathbf{G}_{kg}^{\intercal} \otimes \mathbf{I}_3)^{\intercal} \tag{12}$$

$\mathbf{S}_{f_g}(j\omega)$ is generally for each ω a full matrix. A reduction of the problem size can be obtained when a low correlation of the aerodynamic forces is identified among different parts of the structure. In this case, it can be convenient to divide the structure in correlated parts and perform the explained procedure on those parts independently. The overall spectrum $\mathbf{S}_{f_g}(j\omega)$ will then be the direct sum (cf. [7, pp. 21-22]) of the spectra of the J correlated parts, $\mathbf{S}_{f_g}^{(1)}(j\omega), \ldots, \mathbf{S}_{f_g}^{(J)}(j\omega)$, i.e. it is a block diagonal square matrix

$$\mathbf{S}_{f_g}(j\omega) = \mathbf{S}_{f_g}^{(1)}(j\omega) \oplus \ldots \oplus \mathbf{S}_{f_g}^{(J)}(j\omega) = \mathrm{diag}(\mathbf{S}_{f_g}^{(1)}(j\omega), \ldots, \mathbf{S}_{f_g}^{(J)}(j\omega)) \tag{13}$$

4 BUFFETING IN MODAL SPACE

The word *buffeting* refers to the aeroelastic response of the structure to an unsteady flow excitation.
Let us consider the spectrum $\mathbf{S}_{f_g}(j\omega)$ of the aerodynamic force distribution on the structural mesh. It is convenient to consider only the fluctuating part of the signals, by removing their steady parts. Mean or steady-state loads are not treated in this paper and they can be added separately to the fluctuating components.
Let us consider the transfer function of the aeroelastic system described in modal space as (cf. [12, p. 71])

$$\mathbf{H}(j\omega) = [-\omega^2\widetilde{\mathbf{M}} + j\omega\widetilde{\mathbf{B}} + (1 + jg)\widetilde{\mathbf{K}} - q_\infty\widetilde{\mathbf{Q}}(Ma, k)]^{-1} \tag{14}$$

By using the (real) modal matrix $\mathbf{\Phi}$, the spectrum of the modal amplitudes is given by

$$\mathbf{S}_\xi(j\omega) = \mathbf{H}(j\omega)\mathbf{\Phi}^{\intercal}\mathbf{S}_{f_g}(j\omega)\mathbf{\Phi}\mathbf{H}(j\omega)^{\dagger} \tag{15}$$

and the spectra of the modal velocities and modal accelerations can be derived from $\mathbf{S}_\xi(j\omega)$ as

$$\mathbf{S}_{\dot{\xi}}(j\omega) = \omega^2\mathbf{S}_\xi(j\omega) \tag{16}$$

$$\mathbf{S}_{\ddot{\xi}}(j\omega) = \omega^2\mathbf{S}_{\dot{\xi}}(j\omega) = \omega^4\mathbf{S}_\xi(j\omega) \tag{17}$$

The spectra of the displacements, velocities and accelerations in the physical space are

$$\mathbf{S}_u(j\omega) = \mathbf{\Phi}\mathbf{S}_\xi(j\omega)\mathbf{\Phi}^{\intercal} \tag{18}$$

$$\mathbf{S}_{\dot{u}}(j\omega) = \mathbf{\Phi}\mathbf{S}_{\dot{\xi}}(j\omega)\mathbf{\Phi}^{\intercal} = \omega^2\mathbf{S}_u(j\omega) \tag{19}$$

$$\mathbf{S}_{\ddot{u}}(j\omega) = \mathbf{\Phi}\mathbf{S}_{\ddot{\xi}}(j\omega)\mathbf{\Phi}^{\mathsf{T}} = \omega^4\mathbf{S}_u(j\omega) \tag{20}$$

Similar approaches to the multi-mode buffeting analysis are followed by several authors of different engineering branches, both using measured and analytic pressure spectra (cf. [13–15]). In order to recover the nodal loads, the mode displacement method can be employed as (cf. [16, pp. 641-650])

$$\mathbf{S}_Y(j\omega) = \mathbf{K}\mathbf{S}_u(j\omega)\mathbf{K}^{\mathsf{T}} \tag{21}$$

The spectrum of the integrated loads is finally obtained by summing up the nodal loads at specific monitoring stations. It can be done by using a transformation matrix $\mathbf{T}$ which rotates the nodal loads in the local coordinate system proper to each monitoring station and integrates the nodal loads

$$\mathbf{S}_{Y_{MS}}(j\omega) = \mathbf{T}\mathbf{S}_Y(j\omega)\mathbf{T}^{\mathsf{T}} \tag{22}$$

The computation of spectra for all the DOFs of the system and for all the frequency steps can result to be a heavy task. When such information is needed only at specific DOFs, one can consider sub-matrices of the modal and stiffness matrices by cancelling the undesired DOFs from the rows of both matrices. By entering these sub-matrices in Eqs. (18), (19), (20) and (21) it is then possible to calculate the auto- and cross-spectra of the displacements, velocities, accelerations and nodal loads relative only to the selected DOFs. If one is exclusively interested in specific terms of the spectra (for instance only auto-spectra at specific DOFs), Eq. (18) can be written as

$$S_{u_{lm}}(j\omega) = \sum_{a=1}^{n}\sum_{b=1}^{n}\Phi_{la}S_{\xi_{ab}}(j\omega)\Phi^{\mathsf{T}}_{mb} \tag{23}$$

relative to the DOFs l and m. Velocities, accelerations and loads can be easily derived from Eq. (23).

Usually we are interested in obtaining integrated load envelopes at specific monitoring stations of the aircraft. For this task, it is not needed to compute the full spectra in Eqs. (18), (21) and (22), but only their covariance matrices (cf. [1, pp. 152-154 and 188-191]). From the covariance matrix of the integrated loads, it is then possible to estimate the maximum and minimum loads of the multivariate random problem, how they combine each other and how they combine with other intermediate values (solving what is called the phasing problem, cf. [6, pp. 97-100], i.e. the problem of defining the simultaneously occurring values of two or more variables).

The covariance matrix of the modal amplitudes is the integral of the spectrum in Eq. (15) (cf. [1, pp. 327-328])

$$\mathrm{Cov}(\boldsymbol{\xi}) = \frac{1}{2\pi}\int_{-\infty}^{+\infty}\mathbf{S}_{\xi}(j\omega)\mathrm{d}\omega \tag{24}$$

The covariance matrices of the physical displacements, nodal loads and integrated loads at specific monitoring stations are then

$$\mathrm{Cov}(\mathbf{u}) = \mathbf{\Phi}\,\mathrm{Cov}(\boldsymbol{\xi})\mathbf{\Phi}^{\mathsf{T}} \tag{25}$$

$$\mathrm{Cov}(\mathbf{Y}) = \mathbf{K}\,\mathrm{Cov}(\mathbf{u})\mathbf{K}^{\mathsf{T}} \tag{26}$$

$$\mathrm{Cov}(\mathbf{Y}_{MS}) = \mathbf{T}\,\mathrm{Cov}(\mathbf{Y})\mathbf{T}^{\mathsf{T}} \tag{27}$$

Denoting with $\boldsymbol{\sigma}_{Y_{MS}}$ the diagonal matrix of the standard deviations of the integrated loads, the maximum and minimum fluctuating loads are then obtained as $\pm U_\sigma\boldsymbol{\sigma}_{Y_{MS}}$. U_σ is a factor, which for buffet problems usually assumes a value of 3 or 3.5 in order that 99.865% or 99.977% of all possible values in a Gaussian process are respectively covered. Denoting with $(\mathbf{Y}_{MS})_0$ the mean or steady-state components of the integrated loads, the maximum and minimum loads

are finally the sum of the mean components respectively with the maximum and minimum fluctuating components

$$\begin{cases} (\mathbf{Y}_{MS})_{max} = (\mathbf{Y}_{MS})_0 + U_\sigma \boldsymbol{\sigma}_{Y_{MS}} \\ (\mathbf{Y}_{MS})_{min} = (\mathbf{Y}_{MS})_0 - U_\sigma \boldsymbol{\sigma}_{Y_{MS}} \end{cases} \tag{28}$$

The correlation matrix of the integrated loads is

$$\mathrm{Cor}(\mathbf{Y}_{MS}) = \boldsymbol{\sigma}_{Y_{MS}}^{-1} \Re(\mathrm{Cov}(\mathbf{Y}_{MS})) \boldsymbol{\sigma}_{Y_{MS}}^{-1} \tag{29}$$

and it defines the linear dependency between the load components. The elements on the main diagonal assume unitary values, since every load is perfectly correlated with itself. The off-diagonal terms are $|\rho_{xy}| \leq 1$. When $|\rho_{xy}| = 1$ the two load components x and y are deterministically linearly dependent. If $\rho_{xy} = 0$ then x and y are uncorrelated, i.e. statistically linearly independent.
The information provided by Eqs. (28) and (29) allows to statistically define appropriate combinations of the values that the integrated load components can assume between their minimum and maximum values at the different locations on the aircraft. These load envelopes, as loci of points with the same probability density, are generally n-dimensional, since they represent combinations of at most three forces and three moments at multiple monitoring stations (even if some components are usually neglected depending on the monitoring station considered, thus simplifying the general problem).

5 DESIGN ENVELOPE FOR COMBINED LOADS AND ITS DISCRETIZATION

In this section we shall investigate the geometrical shape of the design load envelope for $n \geq 2$ Gaussian distributed combined loads. We shall show that for $n = 2$ this envelope is an ellipse, for $n = 3$ an ellipsoid and for $n \geq 4$ an n-dimensional ellipsoid. Furthermore, we shall analytically determine some interesting points on this envelope, namely the points of tangency with a bounding n-orthotope (that is a rectangle for $n = 2$ and a cuboid for $n = 3$) and an additional set of equiprobable combined loads given by the intersections of the space diagonals of the bounding n-orthotope with the envelope. This procedure is recommended in [4, pp. 2-C-16/2-C-19] for gust loads when $n = 2$ but, in principle, one can choose any additional set of points on the envelope, e.g. the vertices of the design envelope.
Finally, the design load envelope will be discretized by a circumscribing convex polytope (a polygon for $n = 2$ and a polyhedron for $n = 3$) by using the above calculated points. The vertices of this polytope will be considered as the new design points, introducing a small conservatism. This is the approach proposed by Hoblit (cf. [6, Chapter 6, pp. 97-114]) for the two-dimensional case, where all the vertices of the circumscribing octagon lie on the bounding rectangle of the ellipse. For the three-dimensional case, we introduce a new approach, which can be easily generalized to the n-dimensional case, $n \geq 2$.

5.1 The two-dimensional case, $n = 2$

When only two load components are important in evaluating the strength of the system, a design load ellipse can be determined, as locus of points of equal probability density (cf. [5]). The system must be able to sustain any combination of loads represented by the points on the ellipse. It is an ellipse since the covariance matrix of the two loads X and Y is positive definite. In general, it can be proved that the covariance matrix is positive semi-definite, but we assume the

correlation coefficient ρ_{xy} of the two random load components X and Y to be different from ± 1. If $\rho_{xy} = \pm 1$, the two load components are linearly dependent and the ellipse degenerates into a segment.
The two-dimensional Gaussian probability density function is given by

$$f(x,y) := \frac{1}{2\pi\sigma_x\sigma_y\sqrt{1-\rho_{xy}^2}} e^{-\frac{1}{2}G_2(x,y)}, \quad -\infty < x, y < +\infty \tag{30}$$

The quadratic form $G_2(x,y)$ is defined as

$$G_2(x,y) := \frac{1}{1-\rho_{xy}^2}\left[\left(\frac{x-x_0}{\sigma_x}\right)^2 - 2\rho_{xy}\left(\frac{x-x_0}{\sigma_x}\right)\left(\frac{y-y_0}{\sigma_y}\right) + \left(\frac{y-y_0}{\sigma_y}\right)^2\right] \tag{31}$$

or in matrix form as

$$G_2(x,y) := (\mathbf{x}-\mathbf{x}_0)^\intercal \mathbf{C}_2 (\mathbf{x}-\mathbf{x}_0) \tag{32}$$

where $\mathbf{x} := [x,y]^\intercal$ is the position vector of a point on the ellipse, $\mathbf{x}_0 := [x_0, y_0]^\intercal$ is the vector of the means or steady-state components and $\mathbf{C}_2$ is the inverse of the symmetric and positive definite covariance matrix $\mathbf{\Sigma}_2$ of the load components X and Y, i.e.:

$$\mathbf{C}_2 := \mathbf{\Sigma}_2^{-1} = \operatorname{diag}(1/\sigma_x, 1/\sigma_y)\, \mathbf{R}_2^{-1} \operatorname{diag}(1/\sigma_x, 1/\sigma_y) \tag{33}$$

Note that $\sigma_x, \sigma_y > 0$, $-1 < \rho_{xy} < 1$ and $\mathbf{R}_2$ is the correlation matrix of the load components X and Y.[1] By means of the translation $\mathbf{x}' := \mathbf{x} - \mathbf{x}_0$ (and writing from now on the new coordinates without primes) the quadratic form $G_2(x,y)$ can be written as

$$G_2(x,y) := \mathbf{x}^\intercal \mathbf{C}_2 \mathbf{x} \tag{34}$$

and the origin of the coordinate system is now the centre of the ellipse.
It can be shown that the ellipse of equal probability has the Cartesian equation

$$\left(\frac{x}{\sigma_x}\right)^2 - 2\rho_{xy}\cdot\frac{xy}{\sigma_x\sigma_y} + \left(\frac{y}{\sigma_y}\right)^2 = 1 \tag{35}$$

or in matrix form

$$Q_2(x,y) := \mathbf{x}^\intercal \mathbf{C}_2' \mathbf{x} = 1 \tag{36}$$

where $\mathbf{C}_2' := \det(\mathbf{R}_2)\mathbf{C}_2$ and $\det(\mathbf{R}_2) > 0$. The design load ellipse lies entirely within the rectangle defined by the lines $x = \pm x_{max}$ and $y = \pm y_{max}$ (see Fig. 1).
In order to determine the points of tangency of the ellipse with the lines $x = \pm x_{max}$ (respectively $y = \pm y_{max}$), we note that the slope at these points is zero (respectively ∞). We obtain the relations

$$\sigma_x = \sqrt{1-\rho_{xy}^2}\cdot x_{max}, \quad \sigma_y = \sqrt{1-\rho_{xy}^2}\cdot y_{max} \tag{37}$$

[1] The standard deviations σ_x and σ_y are not the standard deviations given in the main diagonal of $\boldsymbol{\sigma}_{Y_{MS}}$. In order to build the design load envelope, it is necessary to have the correlation matrix $\mathbf{R}_2$ (given by Eq. (29)) and either the maximum values x_{max} and y_{max} of the fluctuating X and Y loads or their standard deviations (i.e. $\boldsymbol{\sigma}_{Y_{MS}}$). We are interested in keeping the maximum values in the load envelope, which are defined by $\operatorname{diag}(x_{max}, y_{max}) := U_\sigma \boldsymbol{\sigma}_{Y_{MS}}$ and $\operatorname{diag}(-x_{max}, -y_{max}) := -U_\sigma \boldsymbol{\sigma}_{Y_{MS}}$ (see Eq. (28)). Consequently one can determine σ_x and σ_y using Eq. (37) and then the load envelope using Eq. (35) or (36). Geometrically, the points with the coordinates $(\pm\sigma_x, 0)$ are the intercepts of the ellipse with the x-axis and those with coordinates $(0, \pm\sigma_y)$ are the intercepts of the ellipse with the y-axis (see Fig. 1).

and the coordinates of the points of tangency I and J are

$$I(x_{max}, \rho_{xy} y_{max}), \quad J(\rho_{xy} x_{max}, y_{max}) \tag{38}$$

Since the ellipse is symmetric with respect to the origin, it follows that the coordinates of I' and J' are $(-x_{max}, -\rho_{xy} y_{max})$ and $(-\rho_{xy} x_{max}, -y_{max})$. A practical additional set of design points can be obtained by intersecting the second (respectively first) diagonal through the origin $(0, 0)$ and the vertex of the bounding rectangle with coordinates $(x_{max}, -y_{max})$ (respectively (x_{max}, y_{max})). In this way one obtains the design points having the coordinates (see Fig. 2)

$$A\left(\sqrt{\frac{1-\rho_{xy}}{2}} \cdot x_{max}, -\sqrt{\frac{1-\rho_{xy}}{2}} \cdot y_{max}\right), B\left(-\sqrt{\frac{1+\rho_{xy}}{2}} \cdot x_{max}, -\sqrt{\frac{1+\rho_{xy}}{2}} \cdot y_{max}\right) \tag{39}$$

By the symmetry of the ellipse with respect to the origin $(0, 0)$, the coordinates of A' and B' are $(-x_A, -y_A)$ and $(-x_B, -y_B)$.
The following design points are chosen in [4, pp. 2-C-16/2-C-19] (see Fig. 2, blue polygon):

$$I, B', J, A', I', B, J', A \tag{40}$$

These points build an irregular octagon circumscribed by the ellipse, i.e. the octagon lies entirely inside the ellipse and only the points (40) are on the ellipse.
A different approach is to consider an irregular octagon circumscribing the ellipse by taking the intersections of the tangent lines at A, A', B, B' with the lines building the bounding rectangle. In this way one obtains the design points

$$R, S, T, U, R', S', T', U' \tag{41}$$

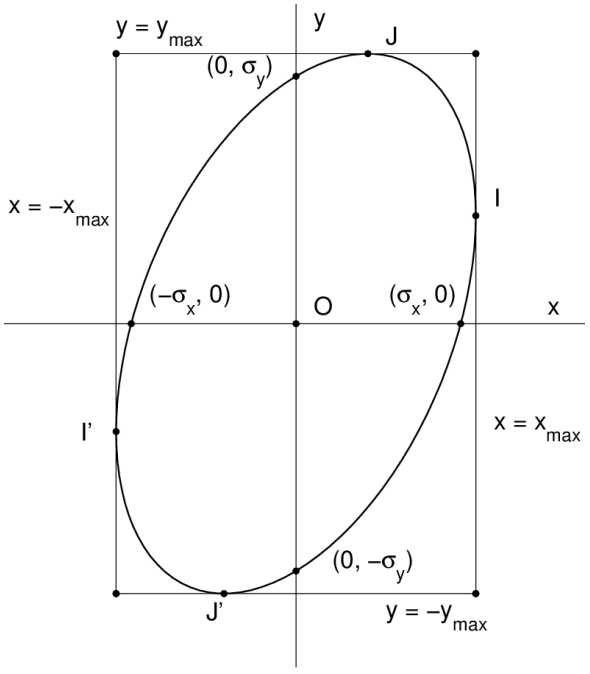

Figure 1: Design load ellipse with bounding rectangle and points of tangency ($\rho_{xy} \geq 0$).

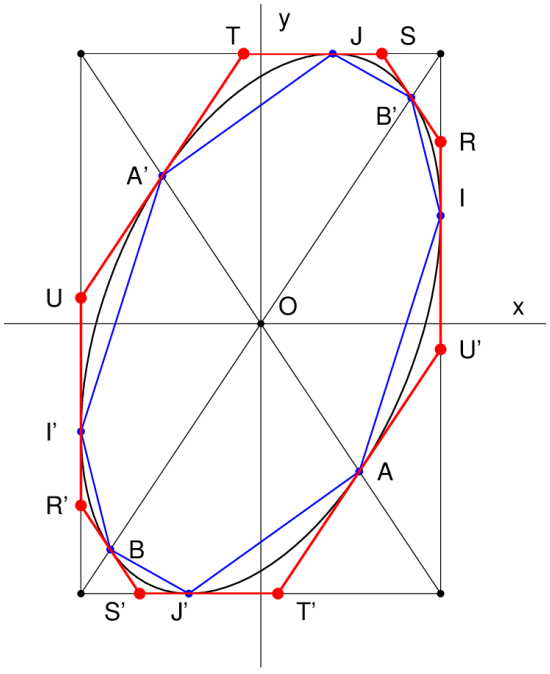

Figure 2: Design load ellipse with inscribed octagon (blue polygon) and circumscribed octagon (red polygon) ($\rho_{xy} \geq 0$).

also proposed by Hoblit (cf. [6, Chapter 6, p.100]).[2] These points build an irregular octagon circumscribing the ellipse, i.e. the ellipse lies entirely inside the octagon and only the points of tangency I, J, I' and J' are on the ellipse (see Fig. 2, red polygon). This choice introduces a small conservatism that can be calculated locally by means of the criticality of the points (41) defined as the ratio

$$cr(P) := \frac{|\overrightarrow{OP}|}{|\overrightarrow{OE}|} \tag{42}$$

where P is an arbitrary point and E is the point of intersection with the ellipse of the line through the origin O and the point P. It is $\overrightarrow{OE} = t\overrightarrow{OP}$, with $t > 0$ and, consequently, $cr(P) = \frac{|\overrightarrow{OP}|}{t|\overrightarrow{OP}|} = \frac{1}{t}$. Inserting the coordinates of E given by $x_E = tx_P$ and $y_E = ty_P$ into the equation of the ellipse one can determine the parameter t. Solving the resulting equation with respect to t it follows

$$cr(P) = \sqrt{\left(\frac{x_P}{\sigma_x}\right)^2 - 2\rho_{xy}\frac{x_P y_P}{\sigma_x \sigma_y} + \left(\frac{y_P}{\sigma_y}\right)^2} = \sqrt{1-\rho_{xy}^2}\cdot d_M(\mathbf{x}_P, \mathbf{0}) = \frac{d_M(\mathbf{x}_P, \mathbf{0})}{d_M(\mathbf{x}, \mathbf{0})} \tag{43}$$

where $d_M(\mathbf{x}_P, \mathbf{0}) := \sqrt{\mathbf{x}_P^\intercal \mathbf{C}_2 \mathbf{x}_P}$ is the *Mahalanobis distance* between the point P with the position vector $\mathbf{x}_P$ and the origin and $d_M(\mathbf{x}, \mathbf{0}) := \sqrt{\mathbf{x}^\intercal \mathbf{C}_2 \mathbf{x}}$ is the Mahalanobis distance between a point on the ellipse with the position vector $\mathbf{x}$ and the origin, since $\mathbf{C}_2 = \mathbf{\Sigma}_2^{-1}$. Note that if the covariance matrix is the identity matrix, the Mahalanobis distance reduces to the Euclidean distance.

5.2 The three-dimensional case, $n = 3$

When three load components are important in evaluating the strength of the system, a design load ellipsoid can be determined as locus of points of equal probability density. The system must be able to sustain any combination of loads represented by the points on the ellipsoid. As in the two-dimensional case, we assume that the correlation coefficients ρ_{xy}, ρ_{xz} and ρ_{yz} are different from ± 1.
The three-dimensional Gaussian probability density function is given by

$$f(x, y, z) := \frac{\sqrt{\det(\mathbf{C}_3)}}{(2\pi)^{3/2}} e^{-\frac{1}{2}G_3(x,y,z)}, \quad -\infty < x, y, z < +\infty \tag{44}$$

where the quadratic form $G_3(x, y, z)$ is defined by

$$G_3(x, y, z) := (\mathbf{x} - \mathbf{x}_0)^\intercal \mathbf{C}_3 (\mathbf{x} - \mathbf{x}_0) \tag{45}$$

and $\mathbf{C}_3$ is the inverse matrix of the symmetric and positive definite covariance matrix $\mathbf{\Sigma}_3$ of the loads X, Y, Z, i.e.:

$$\mathbf{C}_3 := \mathbf{\Sigma}_3^{-1} = \operatorname{diag}(1/\sigma_x, 1/\sigma_y, 1/\sigma_z)\, \mathbf{R}_3^{-1} \operatorname{diag}(1/\sigma_x, 1/\sigma_y, 1/\sigma_z) \tag{46}$$

Moreover, $\mathbf{x} := \left[x, y, z\right]^\intercal$ is the position vector of a point of the ellipsoid, $\mathbf{x}_0 := \left[x_0, y_0, z_0\right]^\intercal$ is the vector of the means or steady-state components, $\mathbf{R}_3$ is the correlation matrix of the loads

[2] The points have coordinates $R\left(x_{max}, \left(\sqrt{2(1+\rho_{xy})} - 1\right) y_{max}\right)$, $S\left(\left(\sqrt{2(1+\rho_{xy})} - 1\right) x_{max}, y_{max}\right)$, $T\left(\left(1 - \sqrt{2(1-\rho_{xy})}\right) x_{max}, y_{max}\right)$, $U\left(-x_{max}, \left(\sqrt{2(1-\rho_{xy})} - 1\right) y_{max}\right)$ and by the symmetry with respect to the origin one obtains R', S', T' and U'.

X, Y, Z, $\sigma_x, \sigma_y, \sigma_z > 0$ and $-1 < \rho_{xy}, \rho_{xz}, \rho_{yz} < 1$. As in the case $n = 2$, it is convenient to make the translation $\mathbf{x}' := \mathbf{x} - \mathbf{x}_0$ in order to have the centre of the ellipsoid at the origin. By means of this transformation (and writing the new coordinates without primes), the design load ellipsoid can be expressed by the Cartesian equation

$$Q_3(x, y, z) := \mathbf{x}^\mathsf{T} \mathbf{C}_3' \mathbf{x} = 1 \tag{47}$$

where $\mathbf{C}_3' := \det(\mathbf{R}_3)\mathbf{C}_3$ and $\det(\mathbf{R}_3) > 0$. In three-dimensional space the equation (47) represents in general a quadric surface (in our case an ellipsoid, since the covariance matrix has been assumed to be positive definite and therefore also the inverse is positive definite) with centre in the origin $(0, 0, 0)$. It lies entirely within the rectangular parallelepiped (or cuboid) defined by the planes $x = \pm x_{max}, y = \pm y_{max}$ and $z = \pm z_{max}$.
In order to determine the points of tangency of the ellipsoid with the circumscribing rectangular parallelepiped, we could proceed as in the two-dimensional case. However, it is easier (especially for the multidimensional case $n \geq 3$) to proceed in the following way.
Let first calculate the normal vector of the ellipsoid at each point given by $\mathbf{n} = \frac{1}{2}\nabla Q_3 = \mathbf{C}_3' \mathbf{x}$. Let I be the point of tangency of the ellipsoid with the plane $x = x_{max}$, J the point of tangency with the plane $y = y_{max}$ and K the point of tangency with the plane $z = z_{max}$. Then, these points are given by the equations

$$\mathbf{C}_3' \mathbf{x}_I = \mu_1 \mathbf{e}_1, \quad \mathbf{C}_3' \mathbf{x}_J = \mu_2 \mathbf{e}_2, \quad \mathbf{C}_3' \mathbf{x}_K = \mu_3 \mathbf{e}_3 \tag{48}$$

where $\mathbf{x}_I := \left[x_I, y_I, z_I\right]^\mathsf{T}$, $\mathbf{x}_J := \left[x_J, y_J, z_J\right]^\mathsf{T}$ and $\mathbf{x}_K := \left[x_K, y_K, z_K\right]^\mathsf{T}$ are the position vectors of the points I, J and K, μ_1, μ_2 and μ_3 are real numbers (not needed for our investigation) and $\mathbf{e}_1$, $\mathbf{e}_2$, and $\mathbf{e}_3$ are the unit vectors in direction of the x-, y- and z-axes. The Eqs. (48) express that $\mathbf{e}_1$ and $\mathbf{C}_3' \mathbf{x}_I$ are two normal vectors to the plane $x = x_{max}$, $\mathbf{e}_2$ and $\mathbf{C}_3' \mathbf{x}_J$ are two normal vectors to the plane $y = y_{max}$ and $\mathbf{e}_3$ and $\mathbf{C}_3' \mathbf{x}_K$ are two normal vectors to the plane $z = z_{max}$. Knowing that the position vector of the point I is $\mathbf{x}_I = \left[x_{max}, y_I, z_I\right]^\mathsf{T}$, where y_I and z_I have to be determined, one can solve the first vector equation for the unknown μ_1, y_I and z_I obtaining

$$y_I = \rho_{xy} \frac{\sigma_y}{\sigma_x} x_{max}, \quad z_I = \rho_{xz} \frac{\sigma_z}{\sigma_x} x_{max} \tag{49}$$

Exactly in the same way, we compute the coordinates of the point of tangency J with the plane $y = y_{max}$ obtaining from the second equation of (48) with $y_J = y_{max}$

$$x_J = \rho_{xy} \frac{\sigma_x}{\sigma_y} y_{max}, \quad z_J = \rho_{yz} \frac{\sigma_z}{\sigma_y} y_{max} \tag{50}$$

and those of the point of tangency K with the plane $z = z_{max}$ obtaining from the third equation of (48) with $z_K = z_{max}$

$$x_K = \rho_{xz} \frac{\sigma_x}{\sigma_z} z_{max}, \quad y_K = \rho_{yz} \frac{\sigma_y}{\sigma_z} z_{max} \tag{51}$$

The standard deviations σ_x, σ_y and σ_z can be determined by noting that the coordinates of I, J and K satisfy the equation (47). Thus substituting the coordinates of I, J and K into (47), one obtains after some lengthy algebraic simplifications the equations

$$\sigma_x = \sqrt{\det\left(\mathbf{R}_3\right)} \cdot x_{max}, \quad \sigma_y = \sqrt{\det\left(\mathbf{R}_3\right)} \cdot y_{max}, \quad \sigma_z = \sqrt{\det\left(\mathbf{R}_3\right)} \cdot z_{max} \tag{52}$$

Finally, with these values we obtain from (49), (50) and (51) the coordinates of I, J and K:

$$I(x_{max}, \rho_{xy} y_{max}, \rho_{xz} z_{max}), \quad J(\rho_{xy} x_{max}, y_{max}, \rho_{yz} z_{max}), \quad K(\rho_{xz} x_{max}, \rho_{yz} y_{max}, z_{max}) \tag{53}$$

As in the two-dimensional case, the points of tangency I' (with the plane $x = -x_{max}$), J' (with the plane $y = -y_{max}$) and K' (with the plane $z = -z_{max}$) are obtained by the half-turn $\mathbf{x}' = -\mathbf{x}$ since the ellipsoid is symmetric with respect to the origin $(0, 0, 0)$.
As in the case $n = 2$, a set of additional points (in total 6 points for $n = 3$) could be either the intersections of the space diagonals of the cuboid with the ellipsoid or the vertices of the ellipsoid defined by the correlation matrix $\mathbf{R}_3$. The determination of these points for both choices is exactly the same as in the two-dimensional case and, therefore, we can omit the details.
In order to derive a convex polyhedron circumscribing the ellipsoid, one could proceed as in the two-dimensional case by calculating the intersections of the tangent planes at the additional points with the planes of the bounding cuboid. However, the natural generalization of the two-dimensional case has some weaknesses. First, the number of vertices tends to be very large (e.g. 8 for $n = 2$, 24 for $n = 3$, ..., 432 for $n = 6$ and so on), giving too many design points. Secondly, for $n \geq 2$, $n - 1$ of the n coordinates are given by the maximum values, which can be too distant from the design envelope (indeed, in the two-dimensional projections of the ellipsoid all vertices lie on the bounding rectangle of the ellipse). Thirdly, each vertex has a different criticality, introducing different levels of conservatism with respect to the actual loads. For all these reasons, this approach cannot be used for $n \geq 3$.

5.2.1 A new approach for the circumscribing polyhedron

A better approach consists in transforming the ellipsoid to a unit sphere, then in finding a polyhedron, possibly regular, that circumscribes it and, finally, in transforming back both the unit sphere and the polyhedron.
Let $\mathbf{u}^\intercal\mathbf{u} = 1$ be the Cartesian equation of the unit sphere, where $\mathbf{u} := [u_1, u_2, u_3]^\intercal$ is the position vector of a point of the unit sphere. Let $\mathbf{\Phi}$ be the 3×3 orthogonal matrix consisting of the eigenvectors of $\mathbf{C}'_3$ and $\mathbf{\Lambda}_3 := \mathrm{diag}(\lambda_1, \lambda_2, \lambda_3)$ be the diagonal matrix of the eigenvalues of $\mathbf{C}'_3$. Then $\mathbf{C}'_3 = \mathbf{\Phi}\mathbf{\Lambda}_3\mathbf{\Phi}^\intercal$ and the transformation

$$\mathbf{x} = \mathbf{\Phi}\mathbf{\Lambda}_3^{-\frac{1}{2}}\mathbf{u} \tag{54}$$

leads the unit sphere to the ellipsoid of equal probability density. Indeed, from (54) it follows $\mathbf{u} = \mathbf{\Lambda}_3^{\frac{1}{2}}\mathbf{\Phi}^\intercal\mathbf{x}$ and, inserting this expression into the equation of the unit sphere, we obtain the equation of the ellipsoid, as $1 = \mathbf{u}^\intercal\mathbf{u} = \mathbf{x}^\intercal\mathbf{\Phi}\mathbf{\Lambda}_3^{\frac{1}{2}}\mathbf{\Lambda}_3^{\frac{1}{2}}\mathbf{\Phi}^\intercal\mathbf{x} = \mathbf{x}^\intercal\mathbf{\Phi}\mathbf{\Lambda}_3\mathbf{\Phi}^\intercal\mathbf{x} = \mathbf{x}^\intercal\mathbf{C}'_3\mathbf{x}$.
The desired polyhedron has to fulfil at least the following criteria: a) the criticality should be the same for all vertices; b) this criticality (≥ 1) should be as small as possible, in order to efficiently approximate the actual envelope; c) it should have as few vertices as possible and d) the generalization of the coordinates of the vertices in n dimensions, $n \geq 3$, should be as easy and natural as possible. The most regular polyhedra are the 5 Platonic solids whose surfaces are composed of only one type of regular polygons. They are the tetrahedron, the hexahedron (or cube), the octahedron, the dodecahedron and the icosahedron. However, only the icosahedron, with 12 vertices and the criticality $\sqrt{15 - 6\sqrt{5}} \approx 1.2584$ (given as the ratio of the radius of the circumscribed sphere and the radius of the inscribed sphere), is a possible candidate. The other 4 solids have either too many vertices (e.g. 20 for the dodecahedron, which has the same criticality as the icosahedron) or the criticality is too high (e.g. 3 for the tetrahedron and $\sqrt{3} \approx 1.732$ for the hexahedron and octahedron). The 12 vertices of an icosahedron with edge-length 2 and centred at the origin are described by all the cyclic permutations of $[0, \pm 1, \pm\varphi]$, where $\varphi := \frac{1+\sqrt{5}}{2} \approx 1.618$ is the *golden ratio*. The coordinates of the $n \cdot 2^{n-1}$ vertices for $n \geq 4$

are given possibly by all the cyclic permutations of $[0, \pm 1, \pm 1, \ldots, \pm\varphi]$.
The next class of polyhedra is given by the Archimedean solids first enumerated by Archimedes. They are also called *semiregular* convex polyhedra and are composed of regular polygons of at least two types meeting in identical vertices. Apart from the prisms and antiprisms, there are only 13 Archimedean solids (cf. [17, pp. 136-140]). Under these 13 solids there are two with only 12 vertices, namely the truncated tetrahedron with criticality $\sqrt{\frac{11}{3}} \approx 1.9149$ and the cuboctahedron with criticality $\sqrt{2} \approx 1.4142$. Four solids, namely the truncated cube, the truncated octahedron, the snub cube and the small rhombicuboctahedron (or expanded cube) have 24 vertices, the first one with criticality 1.4736, the second 1.291, the third 1.176 and the fourth $\sqrt{7-4\sqrt{2}} \approx 1.1589$. All other Archimedian solids have more than 30 vertices (but some of them have a low criticality).
We selected the small rhombicuboctahedron with edge-length 2 as circumscribing regular polyhedron for the design loads ellipsoid (see Fig. 3). This solid can be obtained either by expansion of a cube or can be constructed as the convex hull of the 24 vertices given by all distinct permutations of $[\pm 1, \pm 1, \pm(1+\sqrt{2})]$. It has 26 faces (8 triangular and 18 square faces) and 24 identical vertices, with one triangle and three squares meeting at each vertex. By Euler's polyhedron formula $v - e + f = 2$, where v is the number of vertices, e the number of edges and f the number of faces, it follows that the small rhombicuboctahedron has $e = 48$ edges.
In order to circumscribe the unit sphere by a rhombicuboctahedron, we have to normalize the coordinates of the vertices by $(1+\sqrt{2})$, since this value is the radius of the insphere of the rhombicuboctahedron with edge-length 2. This means that all vectors obtained permuting the coordinates $\mathbf{w} := \frac{1}{1+\sqrt{2}}[\pm 1, \pm 1, \pm(1+\sqrt{2})]^\mathsf{T} = [\pm(\sqrt{2}-1), \pm(\sqrt{2}-1), \pm 1]^\mathsf{T}$ lie on the sphere given by $\mathbf{w}^\mathsf{T}\mathbf{w} = 7 - 4\sqrt{2}$. By means of Eq. (54), we obtain from the coordinates of the vertices of the rhombicuboctahedron the design points of the polyhedron circumscribing the ellipsoid as (see Fig. 4)

$$\mathbf{x}_P = \mathbf{\Phi}\mathbf{\Lambda}_3^{-\frac{1}{2}}\mathbf{w} \tag{55}$$

All these design points with position vector $\mathbf{x}_P$ have the same criticality, namely

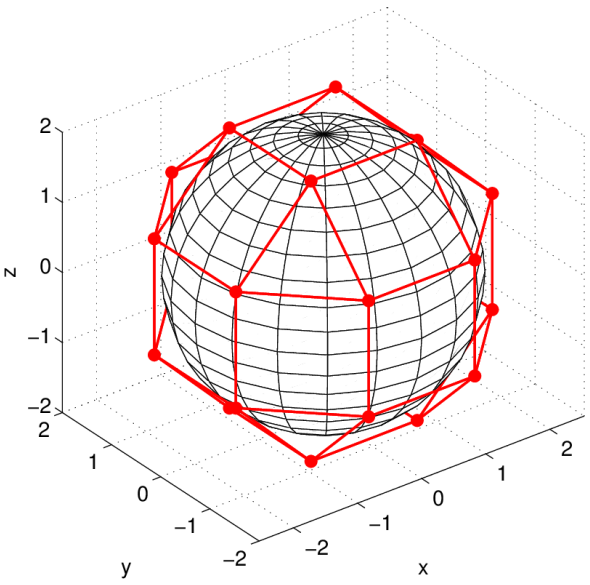

Figure 3: Small rhombicuboctahedron with edge-length 2.

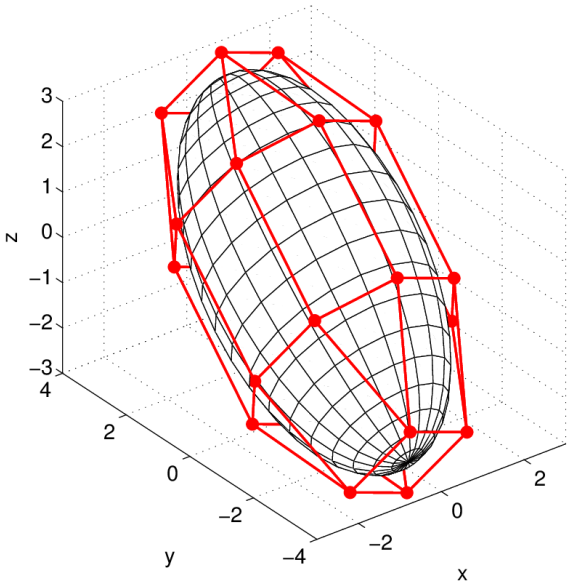

Figure 4: Transformed rhombicuboctahedron circumscribing the ellipsoid of equal probability density. Mahalanobis distance 1.1589.

$$cr(P) = \sqrt{\mathbf{x}_P^{\intercal}\mathbf{C}_3'\mathbf{x}_P} = \sqrt{\det(\mathbf{R}_3)}d_M(\mathbf{x}_P, \mathbf{0}) = \frac{d_M(\mathbf{x}_P, \mathbf{0})}{d_M(\mathbf{x}, \mathbf{0})} \tag{56}$$

where $\mathbf{x}$ is a point on the ellipsoid and $d_M(\mathbf{x}_P, \mathbf{0})$ is the Mahalanobis distance (in the three-dimensional space) between $\mathbf{x}_P$ and the origin.
Eq. (56) can be calculated by using Eq. (54) and it is

$$cr(P) = \sqrt{\mathbf{x}_P^{\intercal}\mathbf{C}_3'\mathbf{x}_P} = \sqrt{\mathbf{w}^{\intercal}\boldsymbol{\Lambda}_3^{-\frac{1}{2}}\boldsymbol{\Phi}^{\intercal}\mathbf{C}_3'\boldsymbol{\Phi}\boldsymbol{\Lambda}_3^{-\frac{1}{2}}\mathbf{w}} = \sqrt{\mathbf{w}^{\intercal}\mathbf{w}} = \sqrt{7 - 4\sqrt{2}} \approx 1.1589 \tag{57}$$

Remark 5.1 *With this new approach it is not necessary any more to calculate additional points in order to construct a circumscribing polyhedron. This is true for all $n \geq 2$.*

5.3 The n-dimensional case, $n \geq 2$

The n-dimensional Gaussian probability density function is given by

$$f(x_1, \ldots, x_n) := \frac{\sqrt{\det(\mathbf{C}_n)}}{(2\pi)^{n/2}} e^{-\frac{1}{2}G_n(x_1,\ldots,x_n)}, \quad -\infty < x_1, \ldots, x_n < +\infty \tag{58}$$

where the quadratic form $G_n(x_1, \ldots, x_n)$ is defined by

$$G_n(x_1, \ldots, x_n) := (\mathbf{x} - \mathbf{x}_0)^{\intercal}\mathbf{C}_n(\mathbf{x} - \mathbf{x}_0) \tag{59}$$

and $\mathbf{C}_n$ is the inverse matrix of the symmetric and positive definite covariance matrix $\boldsymbol{\Sigma}_n$ of the loads $X_1, \ldots, X_n$, i.e.:

$$\mathbf{C}_n := \boldsymbol{\Sigma}_n^{-1} = \operatorname{diag}\left(1/\sigma_{x_1}, \cdots, 1/\sigma_{x_n}\right) \mathbf{R}_n^{-1} \operatorname{diag}\left(1/\sigma_{x_1}, \cdots, 1/\sigma_{x_n}\right) \tag{60}$$

Moreover, $\mathbf{x} := \left[x_1, \ldots, x_n\right]^{\intercal}$ is the position vector, $\mathbf{x}_0 := \left[(x_1)_0, \ldots, (x_n)_0\right]^{\intercal}$ is the vector of the means or steady-state components and $\mathbf{R}_n$ is the correlation matrix of the loads $X_1, \ldots, X_n$. As in the cases $n = 2, 3$ we make the translation $\mathbf{x}' := \mathbf{x} - \mathbf{x}_0$ in order to have the centre of the n-dimensional ellipsoid at the origin. By means of this transformation (and writing the new coordinates without primes) the design load envelope has the form

$$Q_n(x_1, \ldots, x_n) := \mathbf{x}^{\intercal}\mathbf{C}_n'\mathbf{x} = 1 \tag{61}$$

with $\mathbf{C}_n' := \det(\mathbf{R}_n)\mathbf{C}_n$ and $\det(\mathbf{R}_n) > 0$. The design load envelope is an n-dimensional ellipsoid circumscribed by the n-orthotope (also called a *hyperrectangle*) defined by the hyperplanes $x_1 = \pm x_{1_{max}}, \ldots, x_n = \pm x_{n_{max}}$. Note that a 1-orthotope is a segment, a 2-orthotope is a rectangle and a 3-orthotope is a rectangular parallelepiped.
The points of tangency of the n-dimensional ellipsoid with the circumscribing n-orthotope are determined by (see Eq. (48))

$$\mathbf{C}_n'\mathbf{x}_{I_i} = \mu_i \mathbf{e}_i, \quad i = 1, \ldots, n \tag{62}$$

where $\mathbf{x}_{I_1} := \left[x_{1_{I_1}}, \ldots, x_{n_{I_1}}\right]^{\intercal}, \ldots, \mathbf{x}_{I_n} := \left[x_{1_{I_n}}, \ldots, x_{n_{I_n}}\right]^{\intercal}$ are the position vectors of the points $I_1, \ldots, I_n$, and $\mathbf{e}_i$ $(i = 1, \ldots, n)$ is the unit vector in direction of the x_i-axis with the i-th component equal to 1 and zero for all other components. Furthermore, $\mu_1, \ldots, \mu_n$ are real numbers (not needed for our investigation) and both $\mathbf{e}_i$ and $\mathbf{C}_n'\mathbf{x}_{I_i}$ are two normal vectors to the

plane $x_i = x_{i_{max}}$.
Noting that $\mathbf{C}'_n := \det(\mathbf{R}_n)\boldsymbol{\Sigma}_n^{-1}$ we have from (62)

$$\det(\mathbf{R}_n)\boldsymbol{\Sigma}_n^{-1}\mathbf{x}_{I_i} = \mu_i \mathbf{e}_i, \quad i = 1, \ldots, n$$

and solving for $\mathbf{x}_{I_i}$

$$\mathbf{x}_{I_i} = \frac{\mu_i}{\det(\mathbf{R}_n)}\boldsymbol{\Sigma}_n \mathbf{e}_i, \quad i = 1, \ldots, n \tag{63}$$

From these equations, it follows for instance for $i = 1$

$$x_{1_{I_1}} = \frac{\mu_1}{\det(\mathbf{R}_n)}\sigma_{x_1}^2, \quad \ldots, \quad x_{n_{I_1}} = \frac{\mu_1}{\det(\mathbf{R}_n)}\rho_{x_1x_n}\sigma_{x_1}\sigma_{x_n} \tag{64}$$

Since $x_{1_{I_1}} = x_{1_{max}}$, the first equation can be solved with respect to μ_1 obtaining $\mu_1 = \det(\mathbf{R}_n) \cdot x_{1_{max}}/\sigma_{x_1}^2$. Substituting this expression into the last $n-1$ equations and simplifying we obtain

$$x_{2_{I_1}} = \rho_{x_1x_2}\frac{\sigma_{x_2}}{\sigma_{x_1}}x_{1_{max}}, \quad \ldots, \quad x_{n_{I_1}} = \rho_{x_1x_n}\frac{\sigma_{x_n}}{\sigma_{x_1}}x_{1_{max}} \tag{65}$$

Inserting the coordinates $[x_{1_{I_1}}, \ldots, x_{n_{I_1}}]^\intercal$ of the point I_1 into (61) and solving the resulting equation for σ_{x_1} we obtain

$$\sigma_{x_1} = \sqrt{\det(\mathbf{R}_n)} \cdot x_{1_{max}} \tag{66}$$

Repeating these calculations for $i = 2, \ldots, n$, all the coefficients $\mu_i = \det(\mathbf{R}_n) \cdot x_{i_{max}}/\sigma_{x_i}^2$ and all the standard deviations $\sigma_{x_i}, i = 1, \ldots, n$ can be determined

$$\sigma_{x_i} = \sqrt{\det(\mathbf{R}_n)} \cdot x_{i_{max}} \tag{67}$$

Inserting these values into (63) we finally determine the coordinates of the points $I_1, \ldots, I_n$ expressed by means of the correlation coefficients and the maximum values

$$\mathbf{x}_{I_i} = \frac{x_{i_{max}}}{\sigma_{x_i}^2}\boldsymbol{\Sigma}_n \mathbf{e}_i \tag{68}$$

which can be simplified as

$$I_1(x_{1_{max}}, \rho_{x_1x_2}x_{2_{max}}, \ldots, \rho_{x_1x_n}x_{n_{max}}), \quad \ldots, \quad I_n(\rho_{x_1x_n}x_{1_{max}}, \rho_{x_2x_n}x_{2_{max}}, \ldots, x_{n_{max}}) \tag{69}$$

By means of the half-turn $\mathbf{x}' = -\mathbf{x}$, we obtain the remaining points of tangency with the circumscribing n-orthotope, $I'_1, \ldots, I'_n$, since the ellipsoid is symmetric with respect to the origin. As mentioned in remark 5.1, we do not need any more to calculate additional points, the new (conservative) design points are given by the vertices of the n-dimensional rhombicuboctahedron, which can be derived as in Section 5.2.1.
Let us start with the unit n-sphere, $n \geq 2$, and let $\mathbf{u} := [u_1, \ldots, u_n]^\intercal$ be the position vector of a point of the unit n-sphere, $\boldsymbol{\Lambda}_n := \mathrm{diag}(\lambda_1, \ldots, \lambda_n)$ be the diagonal matrix of the eigenvalues of $\mathbf{C}'_n$ and $\boldsymbol{\Phi}$ be the $n \times n$ orthogonal matrix consisting of the eigenvectors of $\mathbf{C}'_n$. Then $\mathbf{C}'_n$ can be factorized as $\mathbf{C}'_n = \boldsymbol{\Phi}\boldsymbol{\Lambda}_n\boldsymbol{\Phi}^\intercal$. The vertices of the n-dimensional small rhombicuboctahedron circumscribing the unit n-sphere are given by all distinct permutations of $\mathbf{w} := \frac{1}{1+\sqrt{2}}[\pm 1, \pm 1, \ldots, \pm(1+\sqrt{2})]^\intercal = [\pm(\sqrt{2}-1), \pm(\sqrt{2}-1), \ldots, \pm 1]^\intercal$ (n coordinates). In total there are $n \cdot 2^n$ vertices lying on the n-sphere given by $\mathbf{w}^\intercal\mathbf{w} = (n-1)(\sqrt{2}-1)^2 + 1 = (3n-2) - 2(n-1)\sqrt{2}$. By means of (54), we obtain the position vectors $\mathbf{x}_P$ of the vertices of the circumscribing polytope as

$$\mathbf{x}_P = \boldsymbol{\Phi}\boldsymbol{\Lambda}_n^{-\frac{1}{2}}\mathbf{w} \tag{70}$$

They all lie on the n-dimensional ellipsoid given by $\mathbf{x}_P^{\mathsf{T}}\mathbf{C}'_n\mathbf{x}_P = \mathbf{w}^{\mathsf{T}}\boldsymbol{\Lambda}_n^{-\frac{1}{2}}\boldsymbol{\Phi}^{\mathsf{T}}\mathbf{C}'_n\boldsymbol{\Phi}\boldsymbol{\Lambda}_n^{-\frac{1}{2}}\mathbf{w} = \mathbf{w}^{\mathsf{T}}\mathbf{w} = (3n-2) - 2(n-1)\sqrt{2}$ and all have the same criticality, namely

$$cr(P) = \sqrt{\mathbf{x}_P^{\mathsf{T}}\mathbf{C}'_n\mathbf{x}_P} = \sqrt{(3n-2) - 2(n-1)\sqrt{2}} \tag{71}$$

that is $\sqrt{4-2\sqrt{2}} \approx 1.08239$ for $n = 2$, $\sqrt{7-4\sqrt{2}} \approx 1.15894$ for $n = 3$, $\sqrt{10-6\sqrt{2}} \approx 1.23074$ for $n = 4$, $\sqrt{13-8\sqrt{2}} \approx 1.29857$ for $n = 5$ and so on.

6 APPLICATIONS

The methods described in the previous sections were applied to two different problems: the delta wing of a fighter aircraft flying in the transonic regime at high angles of attack (Fig. 5) and one of the main landing gear doors of an A320 airplane subjected to the turbulent flow during take-off and landing (Fig. 6). Scope of both studies was the determination of the levels of the structural vibrations at different locations, as well as the calculation of the loads at predefined monitoring stations.

Figure 5: Photo of a modern fighter aircraft (Source: Wikipedia).

Figure 6: Airbus A320-214 with main landing gear doors open. Nose and main landing gears are in transit (Source: Wikipedia).

In the first example, the unsteady pressure distribution on the delta wing was measured during wind-up turn manoeuvres in a flight test campaign. A plain regular grid (namely the aerodynamic grid) was generated within two plain trapezoidal panels (one for the wing and the other for the tip pod) by using a parametric bilinear surface (the hyperbolic paraboloid). The pressures, considered orthogonal to the two panels, were interpolated on the aerodynamic grid and their auto- and cross-spectra were computed (see Fig. 7 and Fig. 8). The pressures were then integrated as described in section 2, obtaining a statically equivalent force distribution on the same grid (Fig. 9). The forces were interpolated on the structural grid of an FEM using surface splines, as described in section 3 and shown in Fig. 10. The stochastic analysis of section 4 was performed, computing auto- and cross-spectra of accelerations at several nodes of the wing as well as loads at all the predefined monitoring stations. As an example, a comparison of numerical (red curve, square markers) and measured (blue curve, circle markers) PSD of the accelerations at the wing tip is shown in Fig. 11. In Fig. 12, the three-dimensional load envelope at the wing root monitoring station is shown with its two-dimensional projections and with the circumscribing transformed rhombicuboctahedron. The vertices of this polyhedron are the desired design load cases for this specific monitoring station.

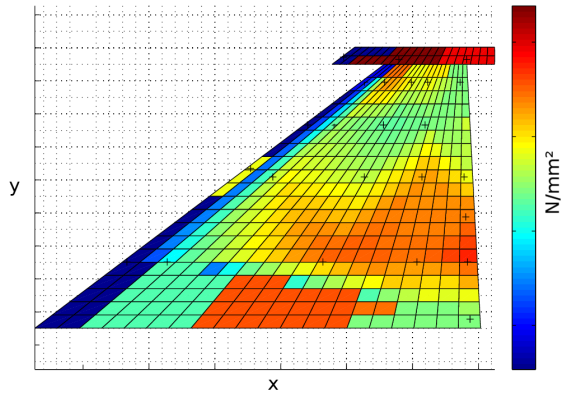

Figure 7: RMS of the pressures measured on the wing upper surface and interpolated on the aerodynamic grid.

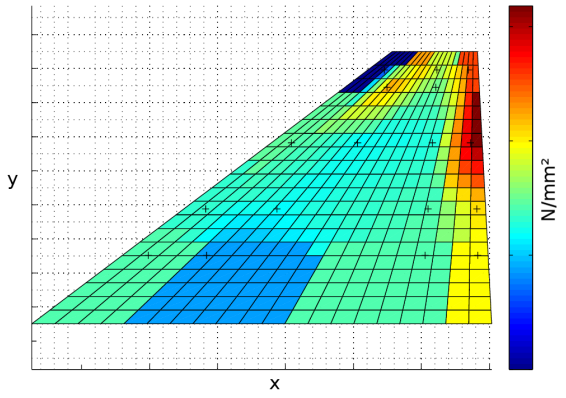

Figure 8: RMS of the pressures measured on the wing lower surface and interpolated on the aerodynamic grid.

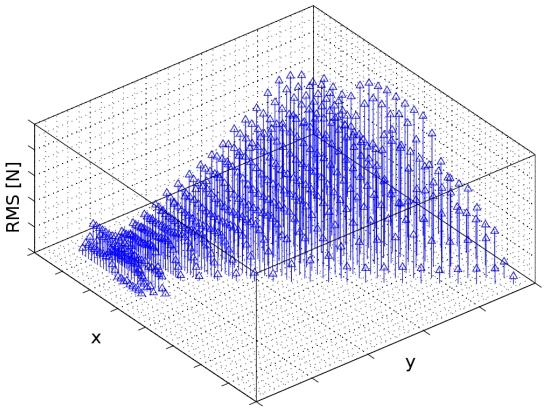

Figure 9: RMS of the forces on the aerodynamic grid of the delta wing.

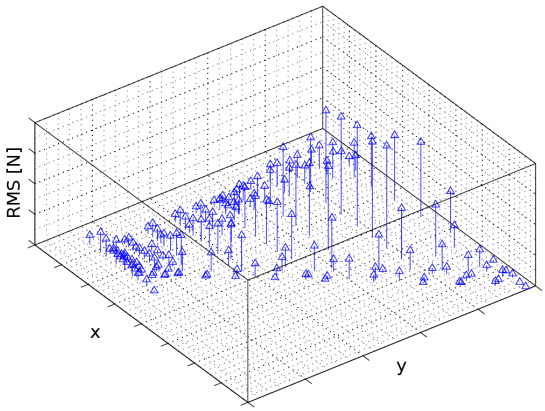

Figure 10: RMS of the forces on the structural grid of the delta wing.

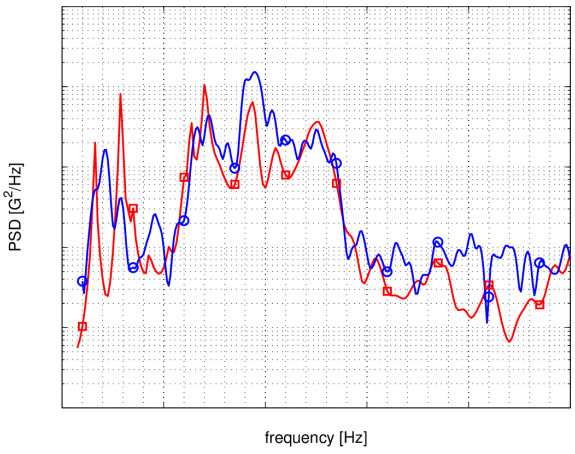

Figure 11: Numerical (red curve, square markers) and measured (blue curve, circle markers) PSD of the accelerations at the wing tip.

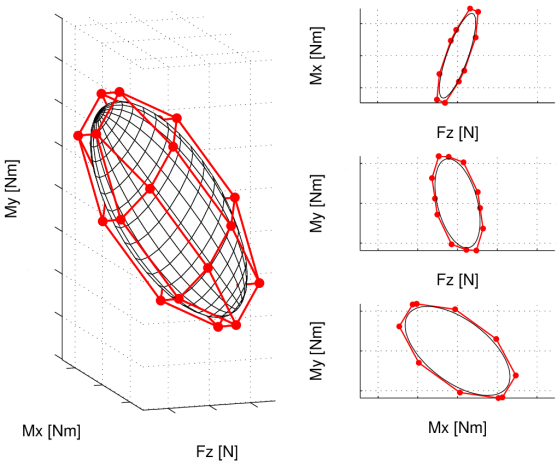

Figure 12: Three-dimensional load envelope and its two-dimensional projections. Wing root monitoring station.

In the second example, the unsteady pressures on one of the main landing gear doors were obtained numerically from CFD. For simplicity, the door was shaped with six panels and the pressures were considered orthogonal to them. The pressures were then interpolated over a regular three-dimensional aerodynamic grid generated within these panels (namely the aerodynamic grid, also in this case created by using a parametric bilinear surface, the hyperbolic paraboloid). Auto- and cross-spectra of the difference between the pressures on the outer and inner surfaces of the door were computed, whose RMS values are shown in Fig. 13. Like in the previous example, the pressures were integrated on the aerodynamic grid (see Fig. 14). Surface splines were then used to interpolate the aerodynamic forces on the grid of an FEM, as shown in Fig. 15. The buffeting analysis described in section 4 was finally performed, computing displacements and accelerations at several nodes of the door in terms of auto- and cross-spectra, as well as the reaction forces at the hinges and at the actuator fitting. The comparison of numerical (red curve, square markers) and measured (blue curve, circle markers) PSD of the actuator loads is shown in Fig. 16.

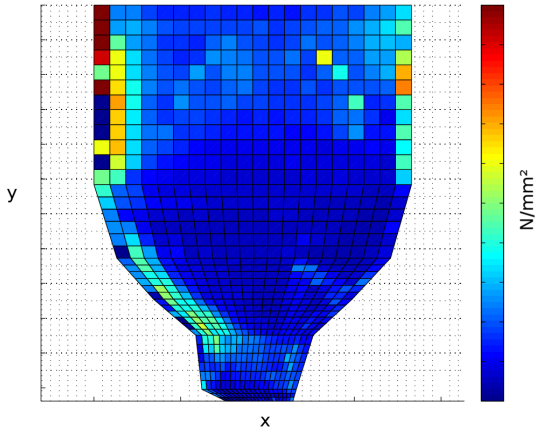

Figure 13: RMS of the pressures on the aerodynamic grid of the main landing gear door. The six panels are shown as unfolded.

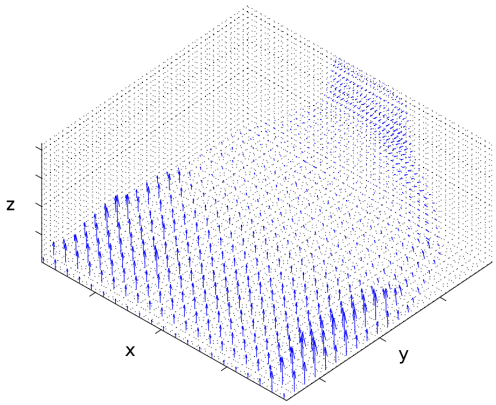

Figure 14: RMS of the forces on the aerodynamic grid of the main landing gear door.

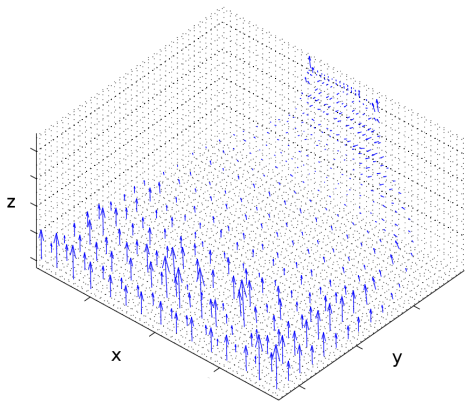

Figure 15: RMS of the forces on the structural grid of the main landing gear door.

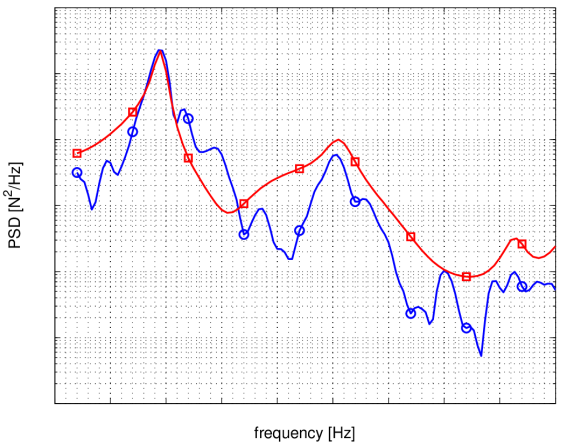

Figure 16: Numerical (red curve, square markers) and measured (blue curve, circle markers) PSD of the actuator loads.

7 CONCLUSIONS

In this paper, a complete method is described for predicting n-dimensional combined loads in the presence of massively separated flows, when both the unsteady pressure distribution and a structural model are available. An n-dimensional load envelope is obtained, which contains equally probable combinations of loads between their minimum and maximum values.
The geometrical shape of the design load envelope is also investigated for $n \geq 2$ Gaussian distributed combined loads, deriving the equation of the n-dimensional ellipsoid and some important points on it, like the points of tangency with the circumscribing n-orthotope, which are the maximum loads.
In order to obtain a finite number of design load cases, a new method for discretizing the n-dimensional ellipsoid is introduced by using a transformed small rhombicuboctahedron. This semiregular polyhedron has the benefit that the criticality, which measures the introduced conservatism with respect to the ellipsoid, is always ≥ 1 and it is the same for all vertices. The small rhombicuboctahedron provides also an excellent compromise in maintaining small both the criticality and the number of design load cases, two requirements which are generally antithetical. Furthermore, the generalization of the coordinates of its vertices to n dimensions, with $n \geq 2$, is straightforward, allowing an easy implementation of the method in computer codes.
As well as for any discretization technique, both the criticality and the number of vertices increase with the number of considered load components. Hence, it is first important trying to reduce the overall number of considered load components (e.g. the shear, the bending and the torsion could be the only loads that one needs to consider for a wing). Secondly, many load components could not be correlated with the others and, for this reason, they could be studied separately (namely different parts of the aircraft could be studied independently, for instance the fin and the wing). Thirdly, once the vertices of the rhombicuboctahedron have been computed, one can still neglect many of the resultant load cases from the analysis. For instance, load components that are highly correlated will be represented by a stretched ellipsoid. Only the most significant among the most correlated load cases could be maintained, since highly correlated load cases, close to a vertex of the stretched ellipsoid, will be almost identical.
The applicability of the methodologies herein described was proved with two different problems. In the first case, the buffeting of the delta wing of a modern fighter aircraft, flying at high angles of attack in the transonic regime, was studied using the unsteady pressure distribution measured during a flight test campaign. In the second case, the buffeting of one of the main landing gear doors of an A320 airplane, subjected to the turbulent flow during take-off and landing, was studied using the unsteady pressures computed numerically from CFD. Both cases show excellent results when compared with test measurements, demonstrating that the same algorithms can be adopted both using numerical data and test measurements.

8 ACKNOWLEDGMENTS

The authors would like to thank Dr. Luca Benassi for having given them the opportunity to study the problem and to present this paper to the conference.

9 REFERENCES

[1] Papoulis, A. (1991). *Probability, Random Variables, and Stochastic Processes*. McGraw-Hill, Inc., 3rd ed.

[2] Guyan, R. J. (1965). Reduction of stiffness and mass matrices. *AIAA Journal*, 3(2), 380.

[3] Albano, E. and Rodden, W. P. (1969). A doublet-lattice method for calculating lift distributions on oscillating surfaces in subsonic flows. *AIAA Journal*, 7(2), 279–285.

[4] European Aviation Safety Agency (23 December 2010). *Certification Specifications for Large Aeroplanes, CS-25, Amendment 10*.

[5] Fuller, J. R. (1982). Boundary excursions for combined random loads. *AIAA Journal*, 20(9), 1300–1305.

[6] Hoblit, F. M. (1988). *Gust Loads on Aircraft: Concepts and Applications*. Washington: AIAA Education Series.

[7] Davis, P. J. (1979). *Circulant Matrices*. Ann Arbor, Michigan: John Wiley & Sons, Reprinted on Demand by University Microfilms International.

[8] Harder, R. L. and Desmarais, R. N. (1972). Interpolation using surface splines. *Journal of Aircraft*, 9(2), 189–191.

[9] Harder, R. L. and Desmarais, R. N. (1972). Reply by authors to W. P. Rodden, J. A. McGrew, and T. P. Kálmán. *Journal of Aircraft*, 9(12), 871.

[10] Rodden, W. P. and McGrew, J. A. (1972). Comment on 'interpolation using surface splines'. *Journal of Aircraft*, 9(12), 869–871.

[11] Duchon, J. (1976). *Constructive Theory of Functions of Several Variables*, chap. Splines Minimizing Rotation-Invariant Semi-Norms in Sobolev Spaces. Oberwolfach: W. Schempp and K. Zeller, Springer.

[12] Rodden, W. P. and Johnson, E. H. (1994). *MSC.Nastran Aeroelastic Analysis Users Guide Version 68*.

[13] Chen, X., Matsumoto, M., and Kareem, A. (2000). Aerodynamic coupling effects on flutter and buffeting responses of bridges. *Journal of Engineering Mechanics*, 20–21.

[14] Farokhi, S., Mirsafian, S., Sherwood, T., et al. (1998). Prediction of antisymmetric buffet loads on horizontal stabilizers in massively separated flows. Melbourne: 21st Congress of International Council of the Aeronautical Sciences.

[15] Pototzky, A. S. and Moses, R. W. (2005). A tail buffet loads prediction method for aircraft at high angles of attack. München: IFASD 2005.

[16] Bisplinghoff, R. L., Ashley, H., and Halfman, R. L. (1996). *Aeroelasticity*. New York: Dover Publications, Inc.

[17] Rouse Ball, W. W. and Coxeter, H. S. M. (1987). *Mathematical Recreations and Essays*. New York: Dover Publications, Inc., 13th ed.

NOMENCLATURE

Acronyms

CFD	computational fluid dynamics
DOF(s)	degree(s) of freedom
FEM	finite element model
PSD	power spectral density
RMS	root-mean-square

Greek Symbols

ω	angular frequency
ω_j	angular natural frequencies
$\mathbf{\Phi}$	modal matrix
ρ	correlation coefficient
σ	standard deviation (root-mean-square if the mean is zero)
$\boldsymbol{\xi}$	modal amplitudes
$\ddot{\boldsymbol{\xi}}$	modal accelerations
$\dot{\boldsymbol{\xi}}$	modal velocities
ζ	ratio of damping to critical damping

Latin Symbols

$\det$	determinant
$\mathbf{C}_n$	inverse of the covariance matrix, $\mathbf{\Sigma}_n^{-1}$
$\widetilde{\mathbf{B}}$	modal damping, $\mathrm{diag}(2\zeta_1\omega_1, \ldots, 2\zeta_n\omega_n)\widetilde{\mathbf{M}}$
c	number of vertices of the r-th cell of the aerodynamic mesh
$\overline{c}$	reference length
Cor, $\mathbf{R}_n$	$n \times n$ correlation matrix
Cov, $\mathbf{\Sigma}_n$	$n \times n$ covariance matrix
cr	criticality
$\mathbf{f}$	nodal forces
g	structural damping
$\mathbf{G}_{kg}$	transformation matrix of the surface spline
$\mathbf{H}$	transfer function
J	number of correlated parts of the structure
j	$\sqrt{-1}$
k	reduced frequency, $\frac{\omega\overline{c}}{2U_\infty}$
$\mathbf{K}$	stiffness
$\widetilde{\mathbf{K}}$	generalized stiffness, $\mathbf{\Phi}^\intercal\mathbf{K}\mathbf{\Phi}$
$\mathbf{M}$	mass
$\widetilde{\mathbf{M}}$	generalized mass, $\mathbf{\Phi}^\intercal\mathbf{M}\mathbf{\Phi}$
Ma	Mach number
n	number of degrees of freedom
$\mathbf{n}$	normal versor
$\mathbf{p}$	nodal pressures
$\widetilde{\mathbf{Q}}$	generalized aerodynamic forces
q_∞	dynamic pressure
R	number of cells of the aerodynamic mesh
$\mathbf{S}$	spectrum
$\mathbf{T}$	transformation matrix
$\ddot{\mathbf{u}}$	physical accelerations
$\dot{\mathbf{u}}$	physical velocities
$\mathbf{u}$	physical displacements
U_∞	free stream velocity
U_σ	factor
Var	variance, $\mathrm{diag}(\mathrm{Cov})$
$\mathbf{Y}$	nodal loads
$\mathbf{Y}_{MS}$	integrated loads

Matrix Notation

$[\,]^+$	Moore-Penrose pseudoinverse
$[\,]^\dagger$	conjugate transpose
$[\,]^\intercal$	transpose
$[\,]^{-1}$	inverse
$\oplus$	direct sum
$\otimes$	Kronecker product
$\mathrm{diag}(\,)$	diagonal matrix

Subscripts and Superscripts

e	expanded
g	indicates relationship to the FEM mesh
k	indicates relationship to the aerodynamic mesh
max	maximum
min	minimum
r	indicates relationship to a cell of the aerodynamic mesh
X, Y, Z	indicates relationship to the global coordinate system
x_r, y_r, z_r	indicates relationship to the local coordinate system of the r-th cell of the aerodynamic mesh. The x_r- and y_r-axis are in the cell plane and the z_r-axis is normal to the cell plane

Other Symbols

$\Im$	imaginary part
$\Re$	real part

COPYRIGHT STATEMENT